



Cite this: *Chem. Commun.*, 2023, 59, 756

Received 27th September 2022,  
Accepted 6th December 2022

DOI: 10.1039/d2cc05305e

[rsc.li/chemcomm](http://rsc.li/chemcomm)

**Epoxidation of dicyclopentadiene (DCPD) is studied on a series of  $\text{TiO}_2$  catalysts using hydrogen peroxide as an oxidant. DCPD derivatives have applications in several areas including polymer, pharmaceutical and pesticide products. The control of selectivity leading to the desired product is important for many of these applications. Using experimental and computational studies, we show that the surface crystalline phases of  $\text{TiO}_2$  play crucial roles not only in the formation of peroxy species but also in the selective epoxidation of two different  $\text{C}=\text{C}$  double bonds in DCPD.**

Given the versatility of the two different double bonds in its chemical structure, dicyclopentadiene (DCPD) is one of the most interesting cyclic olefin compounds. Numerous DCPD derivatives can be found in the pharmaceutical, pesticide, and polymer industries.<sup>1</sup> Amongst the DCPD derivatives, DCPD epoxides find their main uses in adhesives and insulation materials.<sup>2</sup>

Some heterogeneous catalysts have been studied for DCPD epoxidation, such as  $\text{H}_3\text{PW}_{12}\text{O}_{40}$  on SBA-15 and on chloromethylated polystyrene resin,<sup>3,4</sup> and the dispersion of phosphotungstic acid is responsible for the catalytic performance.<sup>4</sup> Metal complexes intercalated in Zn/Al layered double hydroxide structures (Sulfonate-salen- $\text{M}^{\text{III}}$ ,  $\text{M} = \text{Mn}$  or  $\text{Fe}$ ) showed higher activity than  $\text{Fe}$ .<sup>5</sup> Besides the catalytic activity (conversion rate of DCPD), product selectivity is another crucial factor in the epoxidation of DCPD. The epoxidation of DCPD yields two different mono-epoxides (*endo*-4-oxatetracyclo-[6.2.1.0<sup>2,6</sup>0<sup>3,5</sup>]undec-9-ene (**P1**) and *endo*-9-oxatetracyclo-[5.3.1.0<sup>2,6</sup>0<sup>8,10</sup>]undec-3-ene (**P2**)), depending on the location of the epoxide group (in the

## Structure-sensitive epoxidation of dicyclopentadiene over $\text{TiO}_2$ catalysts<sup>†</sup>

Sang-Ho Chung, <sup>‡a</sup> G. Hwan Park, <sup>‡bc</sup> Niels Schukkink, <sup>a</sup> Hyoyoung Lee <sup>\*bc</sup> and N. Raveendran Shiju <sup>\*a</sup>

cyclopentene ring or in the norbornene ring, respectively) (Fig. 1(a)). Due to the difficulty in the product separation unit, the development of a selective epoxidation of DCPD has been encouraged,<sup>6</sup> but the product selectivity typically did not rely on the chemical properties of the metal center.<sup>3–5</sup>

$\text{TiO}_2$  has been widely used as a catalyst for various reactions such as photocatalysis,<sup>7</sup> CO oxidation,<sup>8</sup> and  $\text{H}_2\text{O}_2$  decomposition.<sup>9</sup> In particular, the crystallinity of the  $\text{TiO}_2$  catalysts (anatase and rutile) is responsible for their geometric and electronic properties<sup>10</sup> and plays key roles in view of the product selectivities in the reactions of the decomposition of hydrogen sulphide<sup>11</sup> and the photo-oxidation of water.<sup>12</sup>

Our preliminary results demonstrated that the molecular oxygen (as well as the dissolved oxygen in the liquid phase) could not activate the double bonds of DCPD in methanol at 333 K. For example, insignificant conversion of DCPD (<1%) was obtained at 9 bar of pure oxygen gas in an autoclave. Thus, we studied selective DCPD epoxidation on a series of  $\text{TiO}_2$  catalysts using hydrogen peroxide ( $\text{H}_2\text{O}_2$ ) as an oxidant. Indeed, the epoxidation of cyclic olefin can proceed with  $\text{H}_2\text{O}_2$  in two sequential steps: (i) the formation of peroxy-species on the metal sites and (ii) the oxygen transfer from the surface to an olefin to form an epoxide.<sup>13</sup>

Fig. 1(b) displays the DCPD epoxidation results of two different crystalline phases of  $\text{TiO}_2$ .  $\text{TiO}_2$ -anatase effectively converted DCPD into the related mono-epoxides, showing *ca.* 2 times higher activity than  $\text{TiO}_2$ -rutile ( $C_{\text{DCPD}} = 13\%$  and 7% in 6 h, respectively). The selectivity of the epoxidation products (towards **P1** and **P2**) is greatly influenced by the crystalline phase of the  $\text{TiO}_2$  catalysts. For example, on  $\text{TiO}_2$ -anatase, both **P1** and **P2** were produced with higher selectivity toward **P1** (Table 1). This indicates that the double bond in the cyclopentene ring is preferably reacted on the  $\text{TiO}_2$  anatase phase, which is in line with the previous results over the Ti-incorporated SBA-15 catalyst.<sup>14,15</sup> The DCPD di-epoxide was not observed in this study, suggesting that the epoxidation sites were utilized for the reactant (DCPD) and not occupied by the mono-epoxides, similar to the results of Bhattacharjee *et al.*<sup>5</sup> Interestingly,

<sup>a</sup> Van't Hoff Institute for Molecular Sciences, University of Amsterdam, P.O. Box 94157, 1090 GD Amsterdam, The Netherlands. E-mail: [n.r.shiju@uva.nl](mailto:n.r.shiju@uva.nl)

<sup>b</sup> Center for Integrated Nanostructure Physics, Institute for Basic Science, Sungkyunkwan University, Suwon 440-746, South Korea.

E-mail: [hyoyoung@skku.edu](mailto:hyoyoung@skku.edu)

<sup>†</sup> Department of Chemistry, Sungkyunkwan University, Suwon 440-746, South Korea

<sup>10.1039/d2cc05305e</sup> Electronic supplementary information (ESI) available. See DOI: <https://doi.org/10.1039/d2cc05305e>

<sup>‡</sup> These authors contributed to the manuscript equally.



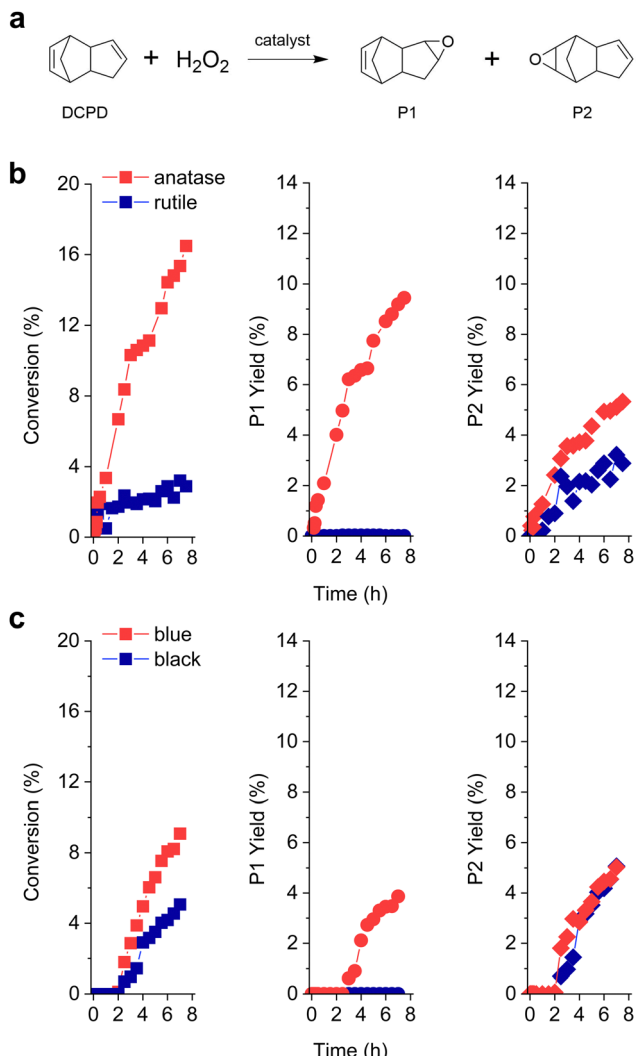


Fig. 1 (a) Reaction scheme of DCPD epoxidation using H<sub>2</sub>O<sub>2</sub> as an oxidant and reaction products **P1** and **P2**. Catalytic performances of different TiO<sub>2</sub> catalysts in the epoxidation of DCPD: (b) TiO<sub>2</sub>-anatase and TiO<sub>2</sub>-rutile; (c) TiO<sub>2</sub>-blue and TiO<sub>2</sub>-black.

Table 1 BET surface area and average pore size for different TiO<sub>2</sub> catalysts, and the catalytic performance results for the epoxidation of DCPD

Catalyst	BET surface area (m <sup>2</sup> g <sup>-1</sup> )	Average pore size (nm)	Normalized activity <sup>a</sup> (mol <sub>DCPD</sub> m <sup>-2</sup> h <sup>-1</sup> )	<i>S</i> <sub>P1/P2</sub>
TiO <sub>2</sub> -anatase	60.8	21.8	28	1.7
TiO <sub>2</sub> -rutile	2.4	16.8	138	0
TiO <sub>2</sub> -blue	58.6	29.2	37	1.1
TiO <sub>2</sub> -black	2.6	16.3	350	0

<sup>a</sup> For TiO<sub>2</sub>-anatase and TiO<sub>2</sub>-rutile, the normalized activity was calculated in 6 h of reaction. For TiO<sub>2</sub>-blue and TiO<sub>2</sub>-black, the activity values were calculated in 8 h, which is *ca.* 6 h from the point of observed conversion.

despite its lower catalytic performance, TiO<sub>2</sub>-rutile solely produced **P2**, *i.e.*, the double bond in the norbornene moiety is selectively reacted to form mono-epoxide.

We further prepared two additional TiO<sub>2</sub> catalysts (TiO<sub>2</sub>-blue and TiO<sub>2</sub>-black),<sup>16–18</sup> and the colors of the catalysts are

attributed to the oxygen vacancies, based on the crystalline phases (anatase and rutile) (Fig. S1, ESI†).<sup>19</sup> At the initial reaction stage (until *ca.* 2 h), no conversion of DCPD was observed over TiO<sub>2</sub>-blue and TiO<sub>2</sub>-black. This suggests that (i) DCPD is not reactive with H<sub>2</sub>O<sub>2</sub> in solution and (ii) a certain delay (or lag-phase) is necessary to initiate DCPD epoxidation over the catalysts with oxygen vacancies. Since the textural properties of TiO<sub>2</sub>-blue and TiO<sub>2</sub>-black are similar to those of TiO<sub>2</sub>-anatase and TiO<sub>2</sub>-rutile, respectively (Table 1 and Fig. S1, S2, ESI,† as also reported by previous works<sup>16–18,20</sup>), we expected that the observed lag-phase is related to the surface oxygen vacancies, which might need to be modified by the oxygen from H<sub>2</sub>O<sub>2</sub>. In terms of the surface area normalized activity (Table 1), TiO<sub>2</sub>-blue and TiO<sub>2</sub>-black showed superior catalytic performance compared to TiO<sub>2</sub>-anatase and TiO<sub>2</sub>-rutile. We expect that the few nanometer layers of the disordered TiO<sub>2</sub> surface<sup>21</sup> can be attributed to the enhanced epoxidation performance. Similarly, the formation of reactive oxygen species is preferred on the amorphous ZrO<sub>2</sub> than the crystalline monoclinic-ZrO<sub>2</sub>.<sup>22</sup> Amorphous Nb<sub>2</sub>O<sub>5</sub> and Ta<sub>2</sub>O<sub>5</sub> also showed higher performance in the catalytic oxidation of glycerol and cyclohexene than their crystalline forms.<sup>23,24</sup> For TiO<sub>2</sub>-blue, both **P1** and **P2** were produced with higher selectivity to **P1** than **P2**. We suggest that the newly formed oxygen functionalities are highly reactive to convert the double bond in the norbornene ring as well as the one in the cyclopentene ring, similar to the fact that the oxygen vacancies are known to be responsible for the altered activity in oxidation reactions.<sup>25</sup> Meanwhile, only **P2** was observed on TiO<sub>2</sub>-black, indicating that the selectivity towards **P1** or **P2** is largely dependent on the surface crystalline phase.

After the epoxidation of DCPD, the color of the spent TiO<sub>2</sub>-anatase catalyst was changed from white to yellow, indicating the formation of the additional surface oxygen functional groups on titania.<sup>26,27</sup> To identify the oxygen functionalities responsible for the catalytic activity, we characterized TiO<sub>2</sub> catalysts with Raman spectroscopy (Fig. 2). For TiO<sub>2</sub>-anatase and TiO<sub>2</sub>-blue, the Raman features at 148, 395, 515 and 630 cm<sup>-1</sup> are attributed to the anatase phase (the modes of E<sub>g</sub>, B<sub>1g</sub>, A<sub>1g</sub> or B<sub>1g</sub>, and E<sub>g</sub>, respectively).<sup>28</sup> Meanwhile, the five Raman bands are observed for TiO<sub>2</sub>-rutile and TiO<sub>2</sub>-black at 140, 235, 445, 610 and 825 cm<sup>-1</sup>, due to the modes of B<sub>1g</sub>, multi-phonon process, E<sub>g</sub>, A<sub>1g</sub> and B<sub>2g</sub>, respectively. After the treatment of TiO<sub>2</sub> with H<sub>2</sub>O<sub>2</sub>, the formation of oxo species on TiO<sub>2</sub> (yellow coloration of TiO<sub>2</sub>) by H<sub>2</sub>O<sub>2</sub> was observed with the possibility of three different forms on the Ti metal centers (oxo, peroxy, and superoxo species).<sup>29</sup> The O–O stretching frequencies are typically observed between 800 and 930 cm<sup>-1</sup>, depending on the coordination with the environment.<sup>30</sup> For example, the Raman band of H<sub>2</sub>O<sub>2</sub> is typically positioned at 880 cm<sup>-1</sup>.<sup>31</sup> On TiO<sub>2</sub>-anatase, the Raman bands of peroxy species were observed at 871 cm<sup>-1</sup>, indicating that the peroxy species are coordinated to the Ti sites (Fig. 3(a)).<sup>32</sup> On the contrary, for TiO<sub>2</sub>-blue, the Raman band of peroxy species was observed at a higher wavenumber (910 cm<sup>-1</sup>) (Fig. 2(b)), related to the perturbation of the chemical structure of the adsorbed molecule on the catalyst surface.<sup>33</sup> For the rutile phase TiO<sub>2</sub> catalysts (*e.g.*, TiO<sub>2</sub>-rutile and TiO<sub>2</sub>-black), however, no additional

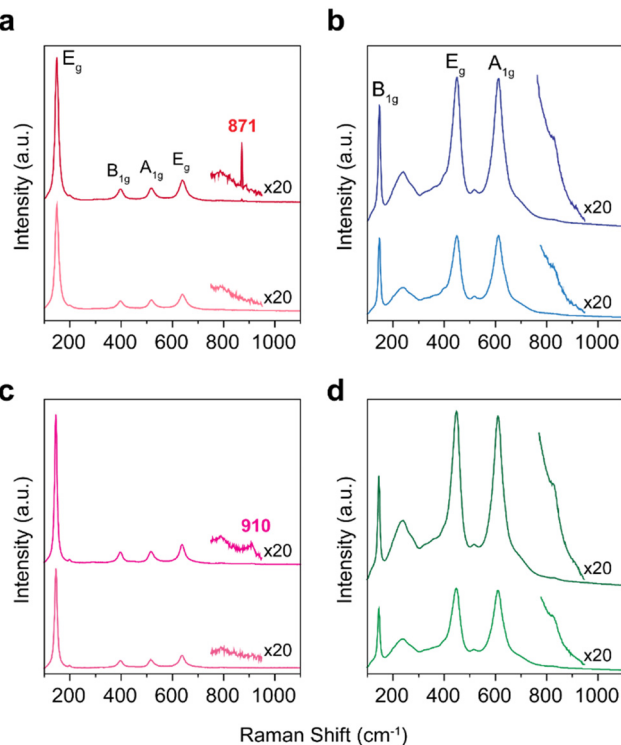


Fig. 2 Raman spectra of  $\text{TiO}_2$  catalysts. (a)  $\text{TiO}_2$ -anatase, (b)  $\text{TiO}_2$ -rutile, (c)  $\text{TiO}_2$ -blue and (d)  $\text{TiO}_2$ -black. In each figure, the Raman spectra of  $\text{H}_2\text{O}_2$  treated samples are displayed on top of the spectra of the untreated samples.

Raman bands are observed after treatment with  $\text{H}_2\text{O}_2$  (Fig. 2(b) and (d)), possibly due to (i) the low surface areas of the rutile phase  $\text{TiO}_2$  catalysts and (ii) the short lifetime of peroxy intermediates on the rutile phase catalysts.<sup>34</sup>

We have explored the reaction pathway of DCPD epoxidation and the selectivity differences among the crystalline  $\text{TiO}_2$  phases using density functional theory (DFT) calculation (Fig. S3 and S4, ESI†). Fig. 3(a) shows the calculated free energy profiles for DCPD epoxidation with  $\text{H}_2\text{O}_2$  catalyzed by the  $\text{TiO}_2$ -anatase and  $\text{TiO}_2$ -rutile. Raman spectroscopy indicates that peroxy species are formed on the surface of  $\text{TiO}_2$ , and the reaction starts from the  $\text{TiO}_2$  surface with adsorbed  $\text{H}_2\text{O}_2$  ( $\text{Ti}-\text{H}_2\text{O}_2^*$ ). Formation of the surface peroxy species ( $\text{Ti}-\text{O}_2^*$ ) proceeds *via* the generation of hydroperoxy compounds. Once the surface of  $\text{TiO}_2$  adsorbed  $\text{H}_2\text{O}_2$ , it firstly generates  $\eta^1$ -coordinated  $\text{Ti}$ -hydroperoxy compounds,  $\text{Ti}-\eta^1(\text{OOH})$ , following the release of a water molecule for  $\text{TiO}_2$ -anatase and  $\text{TiO}_2$ -rutile, which requires +13.0 (Fig. 3(b)) and +19.8 kcal mol<sup>-1</sup> (Fig. 3(c)) at Transition State 1 (TS1), respectively. Subsequently, the thermodynamically more stable  $\eta^2$ -coordinated  $\text{Ti}$ -hydroperoxy compound ( $\text{Ti}-\eta^2(\text{OOH})$ ) is formed. The protonated  $\text{Ti}$ -peroxy species ( $\text{Ti}-\text{O}_2^*$ ) can be formed from  $\text{Ti}-\eta^2(\text{OOH})$  *via* hydrogen transfer to the adjacent  $\text{Ti}$  atom overcoming moderate energy barriers of +13.9 (Fig. 3(b)) and +16.3 kcal mol<sup>-1</sup> (Fig. 3(c)) at TS2 (Fig. 3(a)), respectively. Along the overall reaction steps,  $\text{TiO}_2$ -anatase (Fig. 3(a), red color) has lower free energies than  $\text{TiO}_2$ -rutile (Fig. 3(a), blue color), indicating a higher DCPD conversion rate of  $\text{TiO}_2$ -anatase, which is in good agreement with our experimental results (Fig. 1(b)).

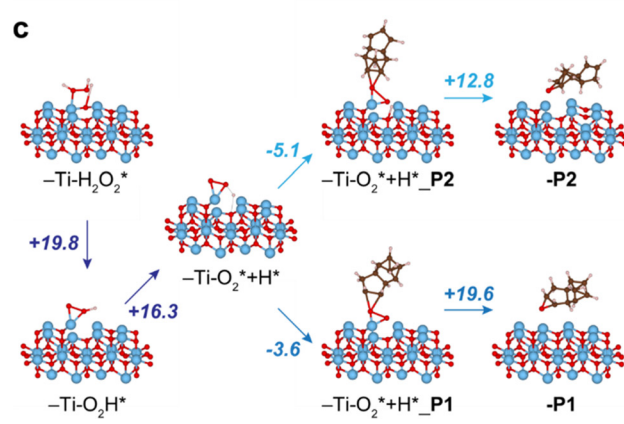
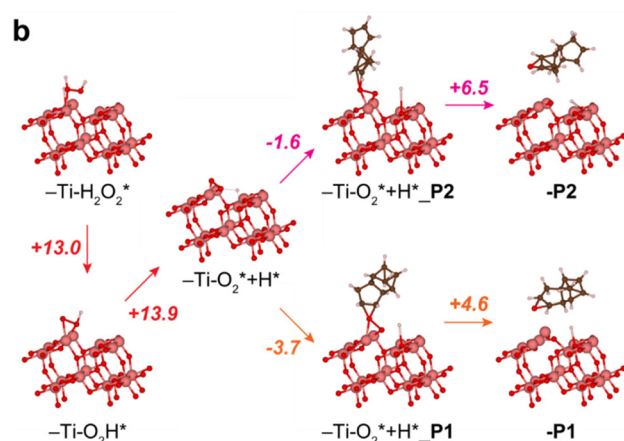
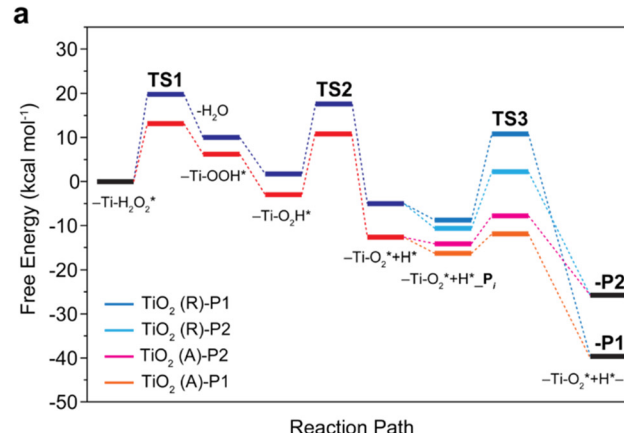


Fig. 3 DFT-calculated free-energy profile (kcal mol<sup>-1</sup>) for the DCPD epoxidation with  $\text{H}_2\text{O}_2$  on  $\text{TiO}_2$ -anatase (b, orange, magenta) and  $\text{TiO}_2$ -rutile (c, navy, blue). The free energies are calculated based on the models in Fig. S5 and S6 (ESI†). The numbers in Fig. 4b and c denote the energy barriers. Coordinates of **-P2** and **-P1** in (b) and (c) are provided in Tables S2–S5, ESI† as representative structures.

The two different C=C bonds in DCPD (cyclopentene or norbornene moiety) have different reactivity to  $\text{TiO}_2$  surface structures. Thus, the selectivity towards **P1** or **P2** strongly depends on the direction of oxygen transfer from  $\text{Ti}$ -peroxy ( $\text{Ti}-\text{O}_2^*$ ). Adsorption of the DCPD molecule on the surface of  $\text{TiO}_2$ -rutile is exothermic for both cyclopentene and norbornene with a very small energy difference (−3.6 and −5.1 kcal mol<sup>-1</sup>



(Fig. 3(c)), respectively). However, O–O bond cleavage with cyclopentene requires a significantly higher energy barrier compared with norbornene (+19.6 and +12.8 kcal mol<sup>-1</sup> (Fig. 3(c)) at TS3 (Fig. 3(a)), respectively). This leads to the selective, one-sided oxygen transfer to the C=C double bond in norbornene, which yields nearly 100% **P2** selectivity. On the other hand, in the case of TiO<sub>2</sub>-anatase, **P1** is preferably formed since the adsorption towards the norbornene moiety requires a higher energy barrier for O–O cleavage than cyclopentene (+6.5 and +4.6 kcal mol<sup>-1</sup>, respectively) (see Fig. 3(b)).

In summary, the surface crystalline phase of TiO<sub>2</sub> catalysts plays a crucial role in selective DCPD epoxidation, not only in the conversion rate of DCPD but also in the product selectivity towards mono-epoxides in cyclopentene and the norbornene moiety. Moreover, the surface oxygen vacancies of TiO<sub>2</sub>-blue and TiO<sub>2</sub>-black are responsible for the lag-phases at the initial reaction stages, indicating that the formation of the surface peroxy functionalities (Ti–O<sub>2</sub><sup>•</sup>) is the rate-determining step.

We acknowledge the Dutch research council (NWO) for the funding (LIFT project 731.017.412), the Institute for Basic Science (IBS-R011-D1), and the Korea Medical Device Development Fund (KMDF\_PR\_20200901\_0004). We thank V. Lachman, N. J. Geels, P. F. Collignon and M.C. Mittelmeijer-Hazeleger (UvA) for the technical support.

## Conflicts of interest

There are no conflicts to declare.

## References

- 1 T. T. P. Cheung, *Kirk-Othmer Encyclopedia of Chemical Technology*, John Wiley & Sons, Inc., Hoboken, NJ, USA, 2001, vol. 2.
- 2 M. Worzakowska, *Polym. Bull.*, 2012, **68**, 775–787.
- 3 R. Gao, Q. Zhu, W. L. Dai and K. Fan, *RSC Adv.*, 2012, **2**, 6087–6093.
- 4 Y. Shen, X. H. Lu, C. C. Wei, X. T. Ma, C. Peng, J. He, D. Zhou and Q. H. Xia, *Mol. Catal.*, 2017, **433**, 185–192.
- 5 S. Bhattacharjee and J. A. Anderson, *J. Mol. Catal. A: Chem.*, 2006, **249**, 103–110.
- 6 M. Sheng and R. Rosenthal, *US Pat.*, 3 631 072, 1971.
- 7 J. Yan, G. Wu, N. Guan, L. Li, Z. Li and X. Cao, *Phys. Chem. Chem. Phys.*, 2013, **15**, 10978–10988.
- 8 J. Li, G. Lu, G. Wu, D. Mao, Y. Guo, Y. Wang and Y. Guo, *Catal. Sci. Technol.*, 2014, **4**, 1268–1275.
- 9 W. F. Huang, P. Raghunath and M. C. Lin, *J. Comput. Chem.*, 2011, **32**, 1065–1081.
- 10 V. Paunović, M. Rellán-Piñeiro, N. López and J. Pérez-Ramírez, *Catal. Today*, 2021, **369**, 221–226.
- 11 R. W. Siegel, *J. Mater. Res.*, 1992, **7**, 2840–2845.
- 12 T. Ohno, D. Haga, K. Fujihara, K. Kaizaki and M. Matsumura, *J. Phys. Chem. B*, 1997, **101**, 6415–6419.
- 13 N. S. Antonova, J. J. Carbó, U. Kortz, O. A. Kholdeeva and J. M. Poblet, *J. Am. Chem. Soc.*, 2010, **132**, 7488–7497.
- 14 Y. C. Lin, C. C. Chang, K. H. Sung, J. F. Lee and S. Cheng, *Microporous Mesoporous Mater.*, 2018, **272**, 276–285.
- 15 P. R. Khoury, J. D. Goddard and W. Tam, *Tetrahedron*, 2004, **60**, 8103–8112.
- 16 Y. Kim, H. M. Hwang, L. Wang, I. Kim, Y. Yoon and H. Lee, *Sci. Rep.*, 2016, **6**, 25212–25221.
- 17 C. T. K. Nguyen, N. Quang Tran, S. Seo, H. Hwang, S. Oh, J. Yu, J. Lee, T. Anh Le, J. Hwang, M. Kim and H. Lee, *Mater. Today*, 2020, **35**, 25–33.
- 18 S. Oh, J. S. J.-H. J. Kim, H. M. Hwang, D. Kim, J. S. J.-H. J. Kim, G. H. Park, J. S. J.-H. J. Kim, Y. H. Lee and H. Lee, *J. Mater. Chem. A*, 2021, **9**, 4822–4830.
- 19 A. Naldoni, M. Altomare, G. Zoppellaro, N. Liu, S. Kment, R. Zbořil and P. Schmuki, *ACS Catal.*, 2019, **9**, 345–364.
- 20 J. Lee, X. Liu, A. Kumar, Y. Hwang, E. Lee, J. Yu, Y. D. Kim and H. Lee, *Chem. Sci.*, 2021, **12**, 9619–9629.
- 21 X. Chen, L. Liu, P. Y. Yu and S. S. Mao, *Science*, 2011, **331**, 746–750.
- 22 K. Sobańska, P. Pietrzyk and Z. Sojka, *ACS Catal.*, 2017, **7**, 2935–2947.
- 23 M. Ziolek, I. Sobczak, P. Decyk, K. Sobańska, P. Pietrzyk and Z. Sojka, *Appl. Catal., B*, 2015, **164**, 288–296.
- 24 M. Ziolek, I. Sobczak, P. Decyk and L. Wolski, *Catal. Commun.*, 2013, **37**, 85–91.
- 25 A. Y. Zhang, T. Lin, Y. Y. He and Y. X. Mou, *J. Hazard. Mater.*, 2016, **311**, 81–90.
- 26 A. H. Boonstra and C. A. H. A. H. A. Mutsaers, *J. Phys. Chem.*, 1975, **79**, 1940–1943.
- 27 J. Zou, J. Gao and Y. Wang, *J. Photochem. Photobiol., A*, 2009, **202**, 128–135.
- 28 W. F. Zhang, Y. L. He, M. S. Zhang, Z. Yin and Q. Chen, *J. Phys. D: Appl. Phys.*, 2000, **33**, 912–916.
- 29 G. L. Gutsev, B. K. Rao and P. Jena, *J. Phys. Chem. A*, 2000, **104**, 11961–11971.
- 30 J. Cho, R. Sarangi, J. Annaraj, S. Y. Kim, M. Kubo, T. Ogura, E. I. Solomon and W. Nam, *Nat. Chem.*, 2009, **1**, 568–572.
- 31 A. A. Mikhaylov, A. G. Medvedev, A. V. Churakov, D. A. Grishanov, P. V. Prikhodchenko and O. Lev, *Chem. – Eur. J.*, 2016, **22**, 2980–2986.
- 32 L. Bonato, M. Virot, T. Dumas, A. Mesbah, P. Lecante, D. Prieur, X. Le Goff, C. Hennig, N. Dacheux, P. Moisy and S. I. Nikitenko, *Chem. – Eur. J.*, 2019, 9580–9585.
- 33 K. Tomobe, E. Yamamoto, D. Kojić, Y. Sato, M. Yasui and K. Yasuoka, *Sci. Adv.*, 2017, **3**, e1701400.
- 34 Á. Ganyecz, P. D. Mezei and M. Kállay, *Comput. Theor. Chem.*, 2019, **1168**, 112607.

